Semarak Climate Science Letters

Journal homepage:
https://semarakilmu.my/index.php/scsl/
ISSN: 3083-9580

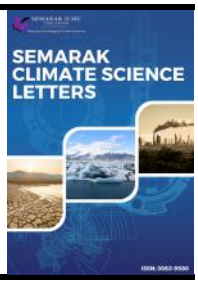


# Two-Phase Flow Regimes characterization via Pressure Heat Map Recognition

Muhammad Sohail[1,3,4], Baafour Nyantekyi-Kwakye[2,*], Adam Jiankang Yang[1], William Pao[3], Muhammad Arif[4], Haris Sheh Zad[4], Ayesha Nadeem[4]

[1] Department of Mechanical Engineering, Dalhousie University, Halifax, Nova Scotia B3H 4R2, Canada
[2] Department of Civil and Resource Engineering, Dalhousie University, Halifax, Nova Scotia B3H 4R2, Canada
[3] Mechanical Engineering Department, Universiti Teknologi PETRONAS, Perak Darul Ridzuan, 32610, Malaysia
[4] Department of Mechanical & Manufacturing Engineering, Pak-Austria Fachhochschule: Institute of Applied Sciences and Technology, Haripur 22621, Pakistan

**ARTICLE INFO**

***Article history:***
Received 29 September 2025
Received in revised form 1 November 2025
Accepted 3 November 2025
Available online 13 November 2025

***Keywords:***
Two-phase flow; heat maps; flow regime prediction; deep learning

**ABSTRACT**

Precise recognition of flow regimes in industrial two-phase flow system is reliant on visual aids. However, opacity of pipe medium poses a significant challenge and presents a pressing need for reliable identification of flow regimes. This study aims to characterize stratified, slug, elongated bubble and dispersed bubble flow by evaluating the performance of four prominent deep learning architectures. Numerical investigation was conducted for pressure signal data collection for individual flow regimes by varying inlet gas and liquid superficial velocities. Frequency with time domain heatmaps were generated from pressure signals and were pre-processed. Data sets were trained, validated and tested using EfficientNetB80, MobileNetV2, Xception, and DenseNet deep learning architectures. Gradient-weighted Class Activation Mapping (Grad-CAM) were created to visualize the targeted features in each architecture. Corresponding performances were evaluated to identify the best deep learning architecture for flow regime characterization from pressure signals heatmaps. MobileNetV2 with accuracy of 92.5% outperformed EfficientNetB80 and DenseNet each with accuracy of 88.46% and Xception having accuracy of 84.62%. Higher rate of confusion in distinguishing between elongated bubble and dispersed bubble flow lead to lower accuracies in the applied lagging models. MobileNetV2 proves to be an effective CNN architecture for identifying two-phase flow regimes from pressure signal heatmaps in industrial systems.

## 1. Introduction

Two-phase flow refers to the simultaneous interactive motion of two phase such as gas and liquid within a conduit [1,2]. Two-phase flow is prevalent in nuclear power plants [3], refrigeration systems [4], chemical industries [5] and energy sector [6]. It is associated with multiple flow patterns including stratified [7], slug [8], elongated bubble [9] and dispersed bubble [10] flow regimes. The precise

* *Corresponding author.*
*E-mail address: BNyantekyi-Kwakye@dal.ca*

https://doi.org/10.37934/scsl.4.1.1427

characterization of these flow patterns is essential for predicting flow characteristics such as pressure drop [11–13], flow regime transitions [14] and integrity of pipeline amidst flow induced vibrations [15]. Prediction of flow regimes have shown notable improvement in accuracy and reliability with the advancement of Machine Learning (ML) models and increased availability of data [16–18]. Traditional classifiers [19], neural networks [20], support vector machines [21], and image processing [22] are few of the ML techniques utilized for flow regime identification in two-phase flow systems. Challenges such as limited accuracy, higher computational intensity, and the need for extensive feature engineering were encountered [23,24]. Brantson *et al.,* [25] employed a Convolutional Neural Network (CNN) to characterize air-water flow regimes in vertical pipes. The findings of the test results show that the supervised CNN model outperforms seven benchmarked supervised machine learning classification models by 99.90% in identifying bubbly, slug, and churn flow patterns. This highlights the CNN's effectiveness in capturing crucial spatial features for accurate classification. A similar study explored the application of a Random Forest (RF) classifier for multi-class flow regime identification in horizontal tubes [26]. Their study discovered that a 5-fold verified KNN model with K = 50 produced the best outcome, with a 97.4% accuracy. Prediction of Six major and four minor flow regimes were evident on the KNN-generated flow maps. The six main regimes are Plug, Slug, and Intermittent at greater liquid superficial velocities, and Annular, Stratified Wavy, and Stratified Smooth at lower fluid superficial velocities. Dispersed Bubbly, Bubbly, Churn, and Wavy Annular flows constitute the four minor flow regions. Umair Khan *et al.,* [16] utilized multiple architectures including Support Vector Machine (SVM) K-Nearest Neighbors (KNN), Artificial Neural Networks (ANN), Gradient Boosting, RF, and Logistic Regression for real-time flow regime detection in horizontal and vertical flow lines. They used Discrete Wavelet Transform (DWT) of pressure signals for pattern classification. The Kernel Fisher Discriminant Analysis (KFDA) achieved the highest clustering efficiency, whereas KNN provided the best classification performance with 90.2% accuracy and strong repeatability.

Ensemble Learning approach for oil-gas flows was explored by Farag *et al.,* [27]. Combining multiple classifiers in ensemble model resulted in 85% accuracy during comparison with actual production. In another study effectiveness of a Deep Belief Network (DBN) for flow regime classification and leakage in horizontal pipelines was investigated [28]. Pressure and velocity data predictor parameters achieved an accuracy of 71% for binary classification in multiphase leak detection and outperformed the statistical techniques. Moreover, in contrast to conventional flow regime maps dependent on limited experimental datasets, Ma *et al.,* [29] applied data-driven learning techniques to predict two-phase flow regimes in LWR and CANDU systems. The Random Forest approach demonstrated superior performance, offering broader applicability and enhanced prediction accuracy. A study on Slovak catchments employed K-means clustering and Principal Component Analysis (PCA) to regionalize low-flow regimes below Q95 across 219 basins ranging from 4 to 500 km² [30]. The optimal number of clusters was identified using the Silhouette coefficient, and an association coefficient was used to assess consistency between clustering and PCA-based pooling.

Convolutional Neural Network (CNN) architectures have been developed to effectively extract spatial features and patterns from input images [31–34]. Krizhevsky *et al.,* [35] marked a significant milestone with image classification accuracy on the ImageNet dataset by introducing AlexNet. VGGNet was proposed for smaller filter sizes by Simonyan et al., [36] for deeper architectures utilization in enhancing performance. Computational and memory resources have been a major issue in dealing with large data sets involving larger numbers of computational layers. Szegedy *et al.,* [37] introduced GoogLeNet (inception) architecture to find a balance between computational resources and accuracy of the model. One of the most occurring issues in deep learning is the vanishing gradient problem [38]. This occurs when gradient of the loss function becomes exceedingly small during backpropagation. Vanishing gradients cause saturation in deep networks with multiple layers and

nonlinear activations, leading to negligible parameter updates and stalled learning. Residual Network (ResNet) mitigated the vanishing gradient problem by introducing residual connections [39]. This allowed efficient gradient propagation and facilitated the training of substantially deeper networks. The availability of large dataset is crucial for achieving significant accuracy of leaning and validation. Industrial systems with limited availability of comprehensive data sources presents considerable hurdle in utilization of deep networks for classifications. Densely connected convolutional networks (DenseNet) is proved to provide higher accuracy with limited training data due to efficient feature reuse through dense layer connections [40].

Studies have highlighted the challenges of limited data availability in industrial settings for classification tasks [22,41,42]. Despite the constraints of a small dataset, EfficientNet-based CNN model was implemented for automated COVID-19 diagnosis from chest images. Using 10-fold stratified cross-validation, the model yielded 99.62% accuracy for binary and 96.70% for multi-class classification. This confirmed EfficientNet's effectiveness in extracting discriminative medical image features with limited data [43]. Efficient parameter usage of EfficientNet's architecture allows for effective learning from small datasets while maintaining high accuracy. In another study facing data scarcity concern, Depth-wise separable convolutions of Xception architecture enable it to efficiently capture spatial features efficiently [44]. This makes Xception particularly adept at learning from small datasets. Ability of Xception to generalize well with limited training samples was emphasized in a study focusing on detection of flow regimes in nuclear reactor coolant systems. The lightweight architecture design and depth-wise separable convolutions of MobileNet make it highly effective for learning from limited training data while maintaining high accuracy [45]. This was supported by a study performed for distinguishing air-water flow regimes in vertical pipes with restricted data availability [22].

The existing methods of flow pattern identification such as, high-speed imaging and signals Fourier analysis depend heavily on manual judgment and resolution limitations [46]. The visual flow regime classification approaches cannot be applied where the flow channel is opaque [47]. The signal Fourier analysis provide limited information about the flow pattern within the pipe specifically in a noisy environment. The challenges posed by opacity in industrial piping and the limited capability of Fourier-based analysis in capturing dynamic regime transitions need to be addressed for enhancing flow patterns identification. Heatmaps produced under varying flow patterns retain both temporal and frequency-domain information creating noise-resilient features for identification of flow regimes without requiring optical access.

This paper aims to investigate the classification of flow regimes using pressure signals obtained from experimentally validated numerical models. The pressure signals representing various flow regimes are processed using Continuous Wavelet Transform (CWT) to generate corresponding heatmaps. These heatmaps serve as input data for four deep learning architectures: EfficientNet, DenseNet, Xception, and MobileNet. Through this comparative study, the performance of each architecture in classifying flow regimes from the pressure signal CWT heatmaps is evaluated, aiming to identify the most effective model for this classification task.

## 2. Methodology

An experimentally validated numerical model was utilized to collect the pressure signals from CFD simulation. The pressure signals accurately represent the dynamic behaviour of various flow patterns by varying gas and liquid superficial velocities. The recorded pressure signals were subjected to Continuous Wavelet Transform (CWT) for generating heatmap images. Each image effectively captures the spatial and temporal characteristics of the corresponding flow regime. Heatmaps

generated offer visual representation of pressure distribution in signals for classification of flow regimes. Four distinct deep learning architectures; EfficientNet, DenseNet, Xception, and MobileNet utilized the produced heatmaps as input data for classification. The effectiveness of each architecture in correctly classifying flow regimes is assessed by a thorough comparative analysis. The objective of this comparative analysis is to determine the layout that performs most effectively and is particularly consistent at identifying flow regimes via deep learning. Performance of each architecture is evaluated using accuracy, precision, recall (sensitivity), F1 score, specificity, Area under the receiver operating characteristic curve (AUC-ROC) and confusion matrix.

### *2.1 Numerical Model*

An experimentally validated numerical model proposed in an earlier study by authors was utilized for pressure signal data collection in the current study [48]. The numerical model encompasses the geometric configuration, computational domain, and results aggregation. Previous studies have established that a length of 81 times the pipe diameter (81D) is necessary to achieve a fully developed flow for a given flow condition [49]. A U-bend geometry consisting of 9.12 meters inlet arm with pipe diameter of 3 inches (76.2 mm) shown in Figure 1, was developed adhering to the dimensions of the experimental setup and achieve a fully developed flow. CFD geometry is divided into 5 individual regions providing additional control over radial and circumferential mesh growth rate. Inlet cross section is divided into central square and outer periphery for air and water inlet boundaries respectively. Pressure signal is collected in each computation for corresponding air and water superficial velocities. Volume of Fluid (VOF) method is employed to capture the air-water phases interface. VOF is known for its high accuracy in capturing interface dynamics and complex free surface phenomena [50]. Accurate estimation of dissipation rate and turbulent viscosity is essential for precise computational modelling of two-phase flow dynamics. The realizable k-ε model was selected because of the revised standard k-ε equations for estimating the dissipation rate and turbulent viscosity [51].

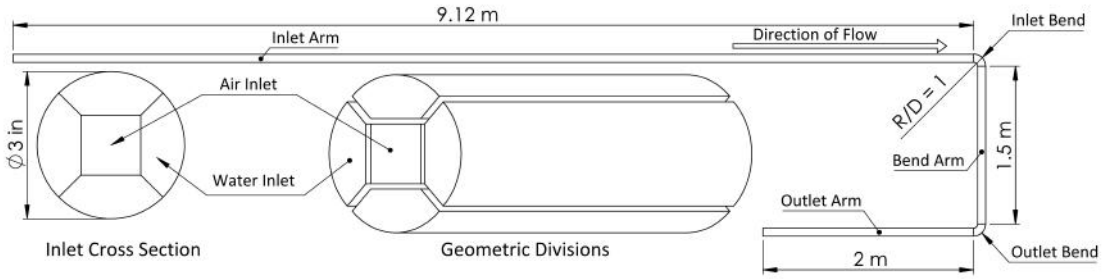


**Fig. 1.** Computational fluid domain geometry [48]

A mesh convergence study was conducted using four mesh resolutions to ensure numerical accuracy while optimizing computational resources [42]. The element size and bias factor were varied to control mesh density and boundary layer capture. Mean dynamic pressure was used as the convergence parameter. Results showed negligible variation between the third (0.545 million elements) and fourth mesh configurations. Therefore, Mesh 3 was selected as it provided a balance between accuracy and computational cost. A time step of 0.001s was chosen to maintain computational stability with a Courant number below 0.5.

### *2.1.1 Boundary Conditions*

The numerical mode defines four individual boundaries including air velocity inlet, water velocity inlet, boundary wall and the pressure outlet. Mandhane flow regime map proposes a map based on gas superficial velocity $J_G$ and liquid superficial velocity $J_L$ [52]. $J_G$ and $J_L$ corresponding to stratified, elongated bubble, slug, and dispersed bubble flow regimes investigated for similar data points and in previous two studies investigated flow induced vibrations and flow induced forces [48,49]. Continuity equations given in Eq. (1) and Eq. (2) were used to calculate the inlet phasal velocities corresponding to $J_G$ and $J_L$. Where inlet velocities of gas and liquid are represented by $V_G$ and $V_L$, respectively. While total cross-sectional area of the pipe is given by $A$.

$$J_G = \frac{A_G V_G}{A} \tag{1}$$

$$J_L = \frac{A_L V_L}{A} \tag{2}$$

### *2.2 Data Pre-processing*

Pressure signals were obtained from the numerical simulations for each flow regime at different combinations of gas and liquid superficial velocities. The collected time-domain pressure signals were converted into frequency–time heatmaps to capture transient and oscillatory behaviors associated with regime transitions. Short-Time Fourier Transform (STFT) was employed to generate heatmaps, with a Hamming window of 256 samples and 50% overlap to ensure temporal resolution of localized frequency variations. The frequency range was limited to 0 - 500 Hz based on dominant fluctuations observed in the pressure spectrum. Generated heatmaps were normalized within the range [0,1] and resized to 224×224 pixels to match the input dimensions required by selected convolutional architectures. Each heatmap represented the dynamic pressure characteristics unique to stratified, slug, elongated bubble, and dispersed bubble flow regimes. To enhance the diversity of training data and reduce model overfitting, several augmentation techniques were applied to the pre-processed heatmaps. Augmentation included random rotation within ±10°, horizontal and vertical shifts of up to 5%, and Gaussian noise insertion with standard deviation of 0.02. These transformations preserved the physical integrity of flow features while improving generalization capability across flow conditions. The augmented dataset expanded the total number of images by approximately fourfold, ensuring balanced representation of all flow regimes during training, validation, and testing. Model development was performed using four state-of-the-art deep learning architectures: EfficientNetB0, MobileNetV2, Xception, and DenseNet. Each model was initialized with ImageNet weights and fine-tuned using the augmented pressure heatmaps. The dataset was split into 70%, 15%, and 15% for training, validation, and testing, respectively. The Adam optimizer was used with an initial learning rate of $10^{-4}$ and batch size of 32. Cross-entropy loss function was employed for multi-class classification. Early stopping was implemented to prevent overfitting by monitoring validation accuracy with a patience of 10 epochs. Gradient-weighted Class Activation Mapping (Grad-CAM) was later used to visualize spatially significant regions influencing the classification decisions in each model.

Previous studies have applied EfficientNet, MobileNet, Xception, and DenseNet for multiphase flow image recognition as discussed in section 1. However, no direct comparison exists for their performance in identifying flow regimes from pressure-based heatmaps. This study compares these

four architectures to determine the most accurate and computationally efficient model for flow regime classification in opaque pipelines via flow pattern heatmaps. The marked differences in architectural complexity across the four CNN models used in this study are presented in Table 1. DenseNet exhibits the deepest structure with 708 layers and 805 connections, indicating a very high level of internal connectivity and feature-reuse. By contrast, MobileNetV2 maintains a relatively modest depth (154 layers) and 163 connections, reflecting its design for efficiency and lower-resource deployment. EfficientNet strikes a mid-range complexity (290 layers / 363 connections), balancing depth and connection count likely due to its compound scaling design. Xception, with approximately 71 layers and an estimated ~95 connections, remains the most compact model of the four; its relatively few connections suggest a lean architecture focused on separable convolutions and efficient parameter usage. In the context of our pressure-signal heat-map classification task, the number of layers and connections may influence both feature extraction capacity and computational cost; the trade-off between model complexity and over-fitting risk is therefore evident from the table.

**Table 01**
Selected number of Layers and Connections of the four models for comparison

| Architectures | Complexity |
|---|---|
| EfficientNet | Layers = 290<br>Connections = 363 |
| DenseNet | Layers = 708<br>Connection = 805 |
| Xception | Layers = 71<br>Connection = 95 |
| MobileNetv2 | Layers = 154<br>Connections = 163 |

### *2.3 Model Evaluation*

Performance of each deep learning model was evaluated using standard classification metrics to ensure robust assessment of flow regime identification accuracy. Accuracy, precision, recall, and F1-score were computed for stratified, slug, elongated bubble, and dispersed bubble flow regimes based on the test dataset. The confusion matrix was generated for each model to visualize the distribution of correct and misclassified samples among the four regimes. In addition, the Receiver Operating Characteristic (ROC) curves and corresponding Area Under Curve (AUC) values were analyzed to quantify classification confidence and separability of flow regimes. The evaluation process also incorporated k-fold cross-validation (k=5) to verify model consistency across different data partitions. Computational efficiency was assessed through model size, training time per epoch, and inference speed per sample to quantify trade-offs between accuracy and computational cost. This comprehensive evaluation enabled comparative performance analysis of EfficientNetB0, DenseNet, Xception, and MobileNetV2 in recognizing two-phase flow regimes from pressure heatmaps.

## 3. Results and Discussion

This section presents a comprehensive analysis of the model behaviour, feature interpretation, and overall classification performance for two-phase flow regime identification. The results are structured to progressively explain how deep learning models extract, interpret, and classify pressure heatmap features corresponding to distinct flow regimes. Section 3.1 examines the representative

feature maps generated from pre-processed pressure heatmaps, highlighting the distinct spatial and temporal characteristics associated with stratified, slug, elongated bubble, and dispersed bubble flows. Section 3.2 provides a detailed Grad-CAM analysis to visualize the attention regions within each deep learning model, emphasizing the specific pressure fluctuation patterns utilized by the networks to distinguish between flow regimes. Subsections 3.2.1 to 3.2.4 focus individually on the four flow regimes, demonstrating how each model identifies regime-specific flow features. Finally, Section 3.3 evaluates the classification performance using quantitative metrics and confusion matrix. The proposed approach identifies stratified, slug, elongated bubble, and dispersed bubble flow regimes with 92.5% accuracy. This approach can monitor flow patterns within opaque pipelines continuously with the integration of pressure transducers. It effectively reduces reliance on visual inspections and improves the pipeline maintenance with a future potential scope for real time monitoring.

### *3.1 Feature Maps*

Feature maps generated from pressure heatmaps reveal distinct visual patterns that correspond to the dynamic characteristics of each two-phase flow regime. Stratified flow, occurring at lower gas and liquid velocities, exhibits smooth transitions and low-frequency variations concentrated near the lower end of the heatmap. These patterns indicate stable phase separation and minimal interfacial disturbance. In contrast, slug flow presents bulky and high-intensity transitions appearing predominantly in the middle region of the heatmap, representing periodic liquid slugs moving through the gas phase and producing strong transient pressure fluctuations. Elongated bubble flow displays vertically stretched peaks distributed horizontally, corresponding to elongated gas bubbles trapped within the continuous liquid phase. As the flow transitions toward dispersed bubble flow, these vertical peaks become thinner and more closely spaced, reflecting the breakup of large, elongated bubbles into numerous smaller dispersed bubbles. The feature maps of dispersed bubble flow are shown in Figure 2.

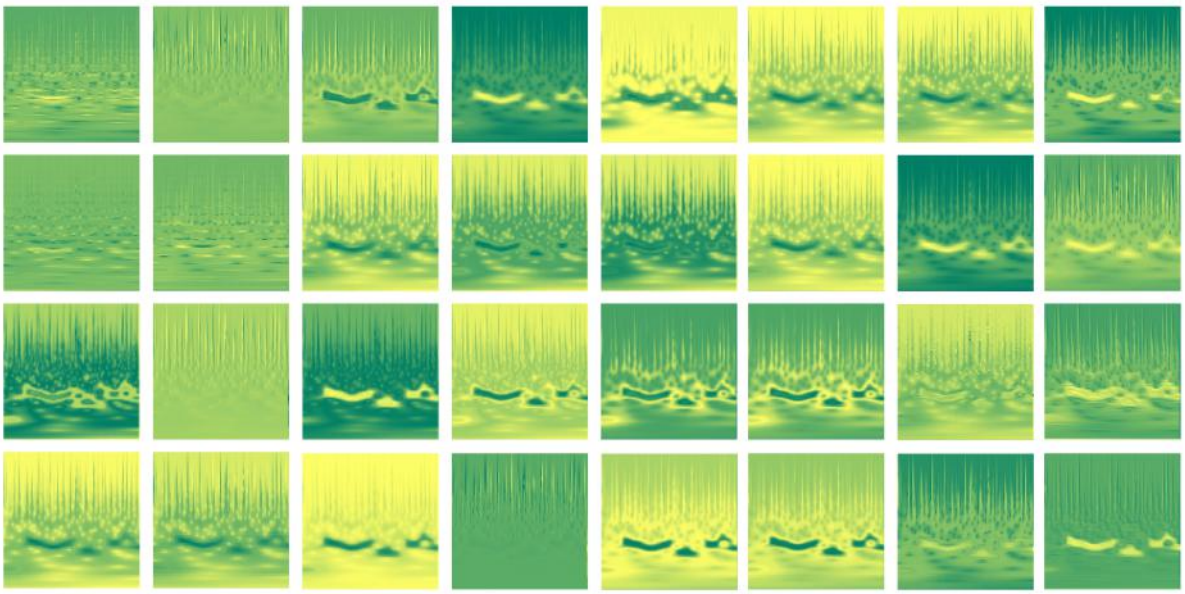

**Fig. 2.** Feature maps of dispersed bubble flows

The convolutional layers of the deep learning models capture these regime-specific spatial–temporal variations at different hierarchical levels. Lower layers emphasize localized gradients and

frequency contrasts, whereas deeper layers encode complex textures and temporal evolution representative of each flow pattern. Visual inspection confirms that the networks effectively learn these discriminative pressure features. Among the evaluated models, MobileNetV2 and DenseNet produced sharper and more interpretable activations across successive layers, suggesting superior efficiency in representing the intrinsic flow characteristics necessary for accurate regime classification.

### *3.2 Grad-CAM Analysis*

Gradient-weighted Class Activation Mapping (Grad-CAM) was employed to interpret and visualize the attention regions within the deep learning models during flow regime classification. Grad-CAM highlights the specific spatial regions in the pressure heatmaps that most strongly influence the model's prediction, thereby providing insight into how each architecture perceives and distinguishes flow features. For each flow regime, the Grad-CAM visualization indicates whether the model focuses on dominant frequency clusters, pressure gradients, or transition zones between phases. Regions of higher activation correspond to pressure instabilities and transient fluctuations that are most relevant to classification. This analysis reveals that MobileNetV2 and DenseNet consistently emphasize physically meaningful regions within the heatmaps, such as slug formation zones and interfacial transitions, while EfficientNetB0 and Xception occasionally display broader and less focused activation patterns. These visual interpretations confirm that the models not only differentiate between flow regimes based on statistical pressure variations but also rely on regime-specific flow dynamics, strengthening confidence in their predictive reliability.

#### *3.2.1 Dispersed Bubble Flow*

The Grad-CAM visualization for dispersed bubble flow highlights the model's focus on high-frequency pressure variations characterized by sharp and closely spaced peaks across the heatmaps as shown in Figure 3. These peaks represent the random and continuous distribution of small gas bubbles dispersed within the liquid phase. The models primarily attend to the sharpness, spacing, and width of these peaks as key indicators for identifying the dispersed bubble regime.

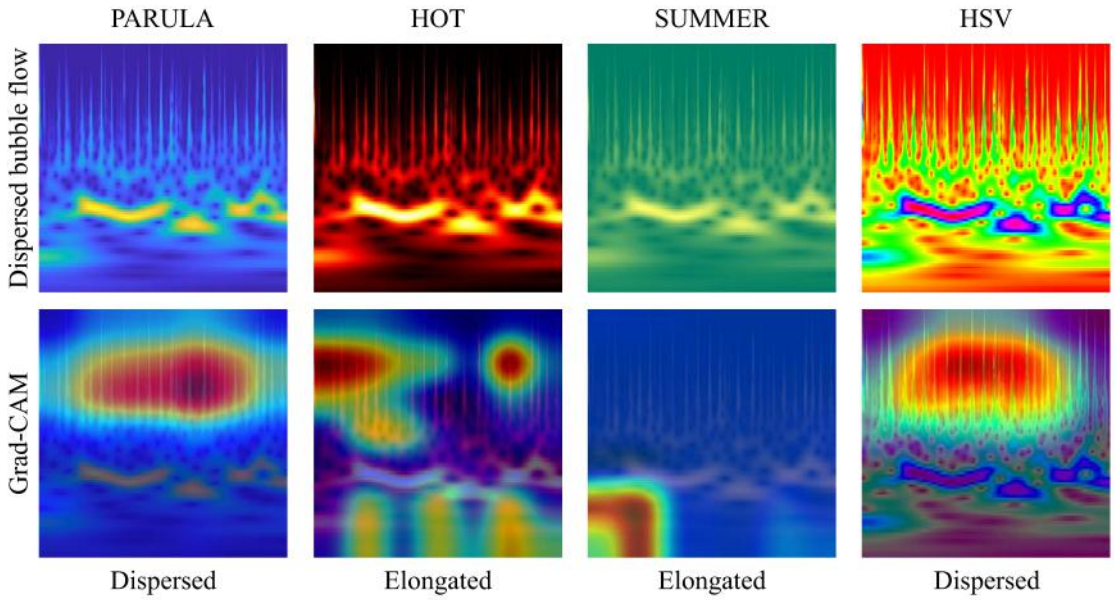


**Fig. 3.** Grad Cam focus on dispersed bubble flow having parula, hot, summer and hsv colormaps

Among the four applied colormaps, the Parula and HSV representations enabled clearer differentiation of these fine-scale features, resulting in correct classification by the models. In contrast, heatmaps generated using the Hot and Summer colormaps produced broader and visually saturated regions, obscuring the fine structural variations between peaks. Consequently, these were misclassified as elongated bubble flow due to the apparent resemblance to elongated gas structures. This observation suggests that the visual contrast and color scaling of the heatmaps significantly influence feature interpretation within deep learning models, emphasizing the importance of optimal colormap selection for accurate dispersed bubble flow recognition.

### *3.2.2 Elongated Bubble Flow*

Grad-CAM visualization for elongated bubble flow demonstrates that all applied models correctly identified the regime across all four-colormaps as presented in Figure 4. The activation regions are concentrated along horizontally distributed vertical peaks within the pressure heatmaps, representing elongated gas bubbles moving through the continuous liquid phase. These peaks exhibit moderate spacing and smoother intensity gradients, distinguishing them from the sharp, densely packed peaks observed in dispersed bubble flow and the bulkier pressure transitions typical of slug flow. The Grad-CAM highlights confirm that the models consistently focused on these vertically extended pressure structures as the primary discriminative feature. The Parula, HSV, Hot, and summer colour maps all preserved the visual contrast necessary to capture the characteristic elongated bubble signatures, indicating that the model's recognition capability for this regime is robust and minimally affected by colormap variations.

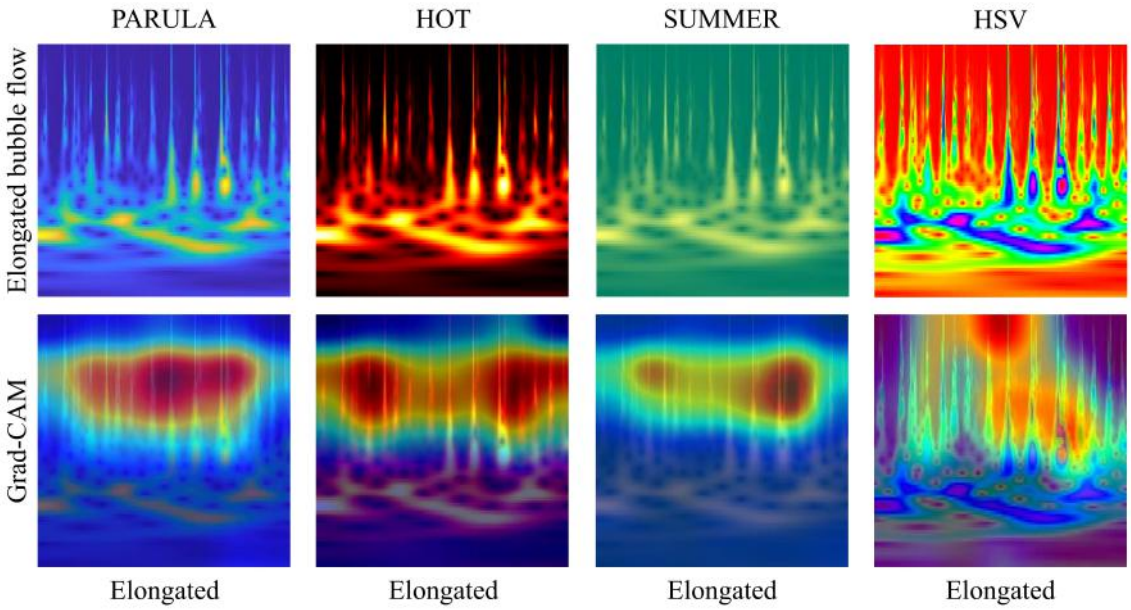


**Fig. 4.** Grad Cam focus on elongated bubble flow having parula, hot, summer and hsv colormaps

### *3.2.3 Slug Flow*

Figure 5 presents the Grad-CAM visualization for slug flow, showing that all four images are correctly identified by the CNN model irrespective of the applied colormap. The highlighted regions indicate that the model primarily focuses on distinct periodic peak formations with large amplitude variations and consistent spacing, which are characteristic of slug flow dynamics. These sharp and

repetitive features correspond to alternating liquid slugs and elongated gas pockets that generate strong, periodic pressure and vibration signatures. The uniform model response across all colormaps confirms the robustness of the CNN in recognizing slug flow features, indicating that colour variations have minimal effect on classification accuracy for this regime.

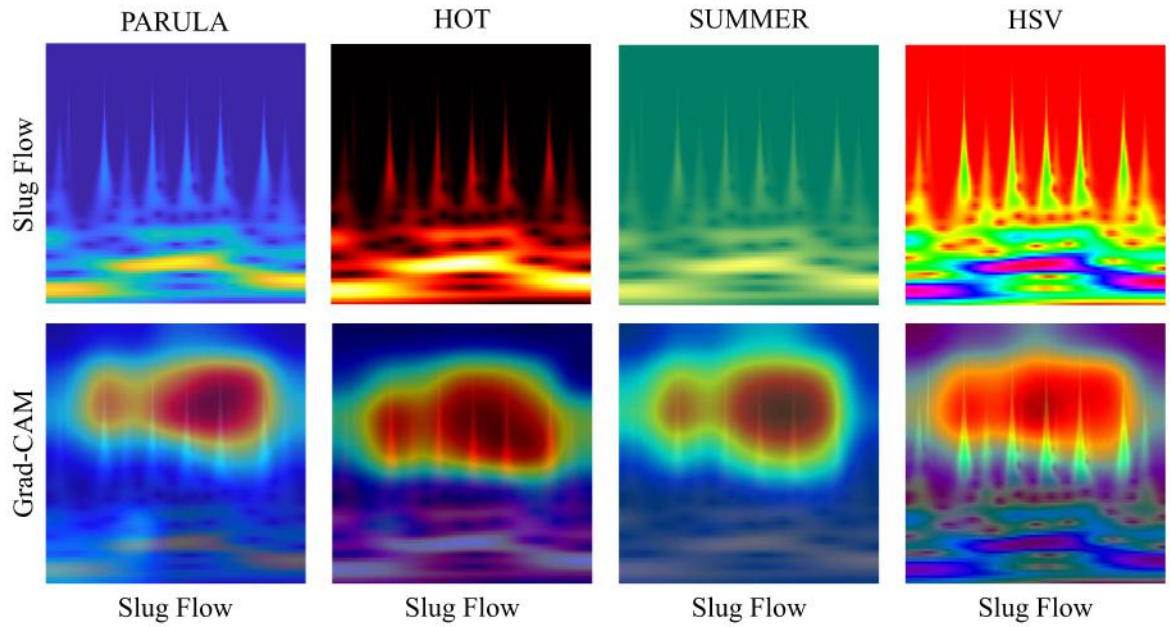


**Fig. 5.** Grad Cam focus on slug flow having parula, hot, summer and hsv colormaps

### *3.2.4 Stratified Flow*

The Grad-CAM visualization for stratified flow, where all images are correctly classified as shown in Figure 6. The model predominantly focuses on the lower region of the CWT images, which corresponds to the low-frequency components of the signal. This region represents the stable liquid layer in stratified flow, where interface disturbances are minimal. The Grad-CAM highlights in this area indicate that the CNN extracts information from the smooth and continuous transitions rather than abrupt intensity changes. Absence of pronounced peaks and the uniform colour variation near the bottom region make stratified flow comparatively easier to identify. This consistent focus pattern confirms that the model associates stratified flow with steady, low-energy fluctuations and a clearly defined interface boundary, distinguishing it from the more dynamic and irregular regimes such as slug or dispersed bubble flows.

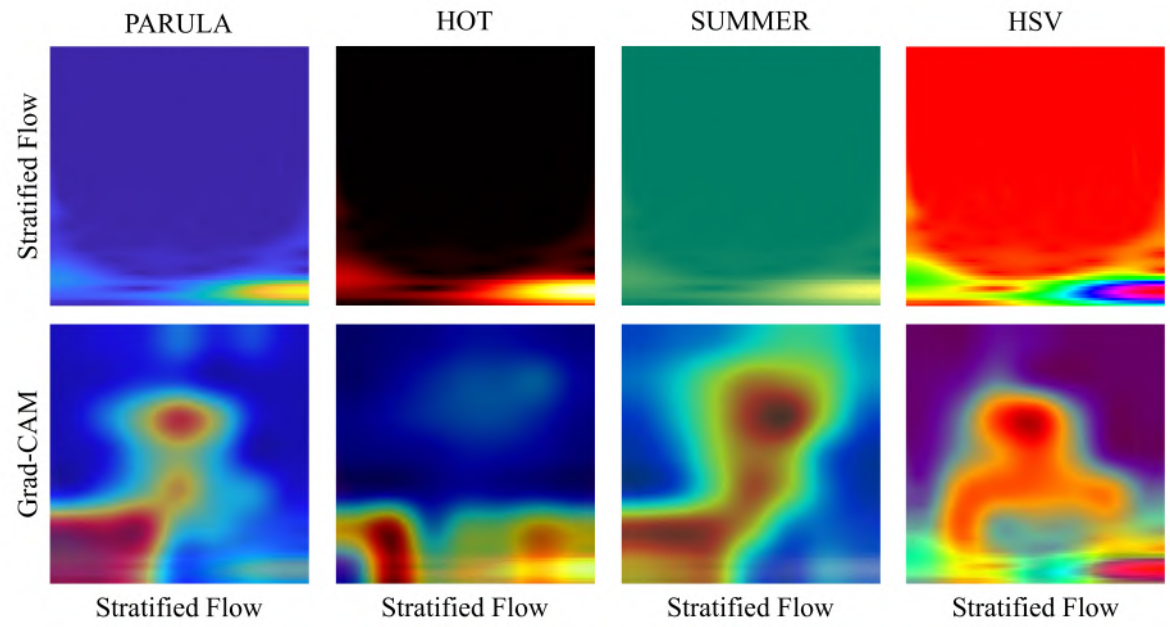


**Fig. 6.** Grad Cam focus on stratified flow having parula, hot, summer and hsv colormaps

### *3.3 Performance Evaluation*

The confusion matrix for the MobileNetV2 classification of two-phase flow regimes is shown in Figure 07. The diagonal entries represent correctly classified samples, while the off-diagonal entries indicate misclassifications. The model correctly identifies all elongated bubble flows (20/20) and most of the slug (19/20) and stratified (19/20) flows. The dispersed bubble flow class shows slightly lower accuracy, with 16 out of 20 samples correctly predicted and 4 misclassified as elongated bubble flow. This confusion primarily occurs because both regimes exhibit similar high-frequency features, but with different intensity and spacing between peaks. The overall distribution of predictions shows strong class separation and minimal overlap, indicating that the CNN effectively distinguishes flow regimes based on spatial-frequency characteristics in the CWT images. The model demonstrates high robustness for elongated, slug, and stratified regimes, while performance can be further improved for dispersed flows through enhanced feature augmentation or refined colormap normalization. Future work can validate the approach using experimental pressure signal data from opaque industrial pipelines. Hybrid deep learning models, such as combining MobileNetV2 with LSTM networks, can be explored to capture both spatial and temporal features of flow regimes. Integration of pressure, vibration, and flow rate sensors can enhance robustness and enable real-time monitoring of two-phase flows.

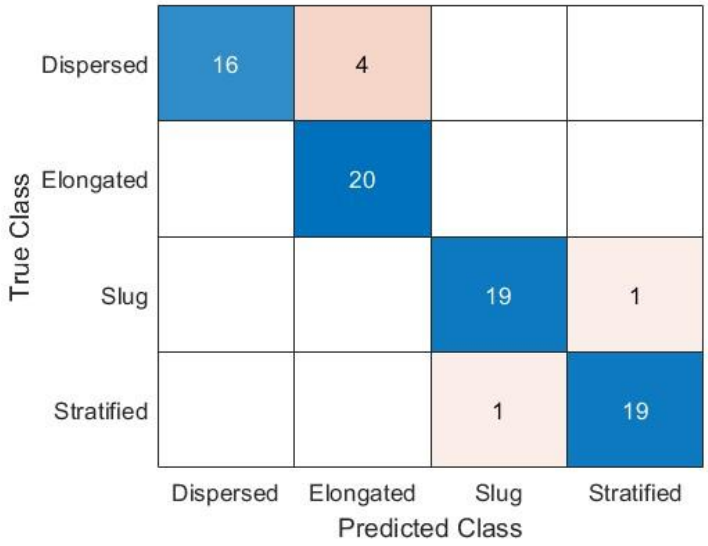


**Fig. 7.** Confusion matrix of MobileNetV2 for flow pattern identification using heatmaps

## 4. Conclusions

The study demonstrated the flow pattern identification capability of four widely deep learning architectures in literatures including EfficientNetB80, MobileNetV2, Xception, and DenseNet trained on CWT heatmaps. Distinct spatial-frequency features were observed in stratified, slug, elongated bubble and dispersed bubble flow CWT feature maps. Grad-CAM visualized the models' emphasis on relevant regions corresponding to the features, such as sharp and closely spaced peaks for dispersed flows, elongated structures for elongated bubbles, and spread pixels over lower regions for stratified flows. MobileNetV2 achieved the highest overall accuracy of 92.5%, outperforming EfficientNetB80 and DenseNet at 88.46% each, and Xception at 84.62%. Misclassification occurred mainly between dispersed and elongated bubble flows due to overlapping spectral features, while slug and stratified flows were classified with over 95% individual accuracies. Overall, the results confirm that the application of CWT with varying colormaps effectively distinguishes flow regimes via MobileNetV2. The discussed approach accurately identifies two-phase flow regimes from pressure CWT heatmaps and offers significant improvement over previously available techniques. The study has future potential of improving real-time industrial monitoring and pipeline maintenance.

## Acknowledgement

The authors would like to acknowledge the financial support from the Universiti Teknologi PETRONAS Institute of Contaminant Management via the Graduate Assistantship scheme and Universiti Teknologi PETRONAS Foundation via YUTP Fundamental Research Grant.

## References

[1] Awad MM, Kazi SN. Two-phase flow. An Overv Heat Transf Phenom 2012:251–340.
[2] Pai S-I. Two-phase flows. vol. 3. Springer-Verlag; 2013.
[3] Poullikkas A. Two phase flow performance of nuclear reactor cooling pumps. Prog Nucl Energy 2000;36:123–30. https://doi.org/10.1016/s0149-1970(00)00007-x.
[4] Cheng L, Liu L. Boiling and two-phase flow phenomena of refrigerant-based nanofluids: Fundamentals, applications and challenges. Int J Refrig 2013;36:421–46. https://doi.org/10.1016/J.IJREFRIG.2012.11.010.
[5] Azbel D, Kemp-Pritchard P. Two-phase flows in chemical engineering 1981:311.
[6] Levy S. Two-phase flow in complex systems. John Wiley & Sons; 1999.

[7] Yih C-S. Stratified flows. Elsevier; 2012.
[8] Taitel Y, Barnea D. Two-Phase Slug Flow. Adv Heat Transf 1990;20:83–132. https://doi.org/10.1016/S0065-2717(08)70026-1.
[9] Roitberg E, Barnea D, Shemer L. Elongated bubble shape in inclined air-water slug flow. Int J Multiph Flow 2016;85:76–85. https://doi.org/10.1016/J.IJMULTIPHASEFLOW.2016.05.011.
[10] Andreussi P, Paglianti A, Silva FS. Dispersed bubble flow in horizontal pipes. Chem Eng Sci 1999;54:1101–7. https://doi.org/10.1016/S0009-2509(98)00289-9.
[11] Shadloo MS, Rahmat A, Karimipour A, Wongwises S. Estimation of pressure drop of two-phase flow in horizontal long pipes using artificial neural networks. J Energy Resour Technol Trans ASME 2020;142. https://doi.org/10.1115/1.4047593/1084716.
[12] Müller-Steinhagen H, Heck K. A simple friction pressure drop correlation for two-phase flow in pipes. Chem Eng Process Process Intensif 1986;20:297–308. https://doi.org/10.1016/0255-2701(86)80008-3.
[13] Zhao TS, Bi QC. Pressure drop characteristics of gas–liquid two-phase flow in vertical miniature triangular channels. Int J Heat Mass Transf 2001;44:2523–34. https://doi.org/10.1016/S0017-9310(00)00282-9.
[14] Hassan I, Vaillancourt M, Pehlivan K. Two-Phase Flow Regime Transitions in Microchannels: A Comparative Experimental Study. Microscale Thermophys Eng 2005;9:165–82. https://doi.org/10.1080/10893950590945049.
[15] Miwa S, Mori M, Hibiki T. Two-phase flow induced vibration in piping systems. Prog Nucl Energy 2015;78:270–84. https://doi.org/10.1016/J.PNUCENE.2014.10.003.
[16] Khan U, Pao W, Pilario KE, Sallih N, Sohail M, Azam H. Real-time automatic flow regime classification and mapping for vertical pipes using dynamic pressure signals. Int J Multiph Flow 2025;189:105252. https://doi.org/10.1016/J.IJMULTIPHASEFLOW.2025.105252.
[17] Hafsa N, Rushd S, Yousuf H. Comparative Performance of Machine-Learning and Deep-Learning Algorithms in Predicting Gas–Liquid Flow Regimes. Process 2023, Vol 11, Page 177 2023;11:177. https://doi.org/10.3390/PR11010177.
[18] Alhashem M, Aramco S. Supervised Machine Learning in Predicting Multiphase Flow Regimes in Horizontal Pipes. Soc Pet Eng - Abu Dhabi Int Pet Exhib Conf 2019, ADIP 2019 2019. https://doi.org/10.2118/197545-MS.
[19] Haase S, Marschner S, Ayubi MM, Lange M. Gas-liquid flow in small channels: Artificial neural network classifiers for flow regime prediction. Chem Eng Process - Process Intensif 2022;180:108687. https://doi.org/10.1016/J.CEP.2021.108687.
[20] Osman E-SA, Fahd K. Artificial Neural Network Models for Identifying Flow Regimes and Predicting Liquid Holdup in Horizontal Multiphase Flow. SPE Prod Facil 2004;19:33–40. https://doi.org/10.2118/86910-PA.
[21] Trafalis TB, Oladunni O, Papavassiliou D V. Two-phase flow regime identification with a multiclassification support vector machine (SVM) model. Ind Eng Chem Res 2005;44:4414–26. https://doi.org/10.1021/IE048973L/ASSET/IMAGES/MEDIUM/IE048973LE00097.GIF.
[22] Azam H, Pao W, Sallih N, Sohail M. Passive flow regime identification based on synchrosqueezing wavelet transform and deep learning. Exp Comput Multiph Flow 2025. https://doi.org/10.1007/S42757-024-0214-1.
[23] Xu H, Tang T, Zhang B, Liu Y. Identification of two-phase flow regime in the energy industry based on modified convolutional neural network. Prog Nucl Energy 2022;147:104191. https://doi.org/10.1016/J.PNUCENE.2022.104191.
[24] Kumar V, Kedam N, Sharma KV, Mehta DJ, Caloiero T. Advanced Machine Learning Techniques to Improve Hydrological Prediction: A Comparative Analysis of Streamflow Prediction Models. Water 2023, Vol 15, Page 2572 2023;15:2572. https://doi.org/10.3390/W15142572.
[25] Brantson ET, Abdulkadir M, Akwensi PH, Osei H, Appiah TF, Assie KR, et al. Gas-liquid vertical pipe flow patterns convolutional neural network classification using experimental advanced wire mesh sensor images. J Nat Gas Sci Eng 2022;99:104406. https://doi.org/10.1016/J.JNGSE.2021.104406.
[26] Manikonda K, Islam R, Obi CE, Hasan AR, Sleiti AK, Abdelrazeq MW, et al. Horizontal Two-Phase Flow Regime Identification with Machine Learning Classification Models. Int Pet Technol Conf IPTC 2022 2022. https://doi.org/10.2523/IPTC-22153-MS.
[27] Farag WA, Aly WHF. Ensemble machine learning-based virtual multiphase flow metering in high gas/oil ratio and water-cut reservoirs. Flow Meas Instrum 2024;100:102737. https://doi.org/10.1016/J.FLOWMEASINST.2024.102737.
[28] Ferroudji H, Al-Ammari WA, Barooah A, Hassan I, Sleiti AK, Gomari SR, et al. A Deep Learning Model for Leakage Identification in Multiphase Flow Systems. SPE Annu Tech Conf Exhib 2025. https://doi.org/10.2118/227979-MS.
[29] Ma Y, Kong D, Zhang J, Wang M, Tian W, Wu Y, et al. Study on flow regime prediction model for water-cooled reactor core based on machine learning algorithms. Ann Nucl Energy 2024;201:110428. https://doi.org/10.1016/J.ANUCENE.2024.110428.
[30] Stevková A, Sabo M, Kohnová S. Pooling of low flow regimes using cluster and principal component analysis.

Slovak J Civ Eng 2012;20:19.
[31] Kattenborn T, Leitloff J, Schiefer F, Hinz S. Review on Convolutional Neural Networks (CNN) in vegetation remote sensing. ISPRS J Photogramm Remote Sens 2021;173:24–49. https://doi.org/10.1016/J.ISPRSJPRS.2020.12.010.
[32] Ma A, Rahmaniar W, Imam Karim Fathurrahman H, Zatu Kusuma Frisky A, Mazhar ul Haq Q. Understanding of Convolutional Neural Network (CNN): A Review. Int J Robot Control Syst 2022;2:739–48. https://doi.org/10.31763/ijrcs.v2i4.888.
[33] Wu J. Introduction to Convolutional Neural Networks 2017.
[34] Chauhan R, Ghanshala KK, Joshi RC. Convolutional Neural Network (CNN) for Image Detection and Recognition. ICSCCC 2018 - 1st Int Conf Secur Cyber Comput Commun 2018:278–82. https://doi.org/10.1109/ICSCCC.2018.8703316.
[35] Alex Krizhevsky, Ilya Sutskever GH. 【AlexNet】ImageNet Classification with Deep Convolutional Neural Networks Alex 2006;8:713–72.
[36] Simonyan K, Vedaldi A, Zisserman A. Deep Inside Convolutional Networks: Visualising Image Classification Models and Saliency Maps. 2nd Int Conf Learn Represent ICLR 2014 - Work Track Proc 2013.
[37] Szegedy C, Liu W, Jia Y, Sermanet P, Reed S, Anguelov D, et al. Going Deeper With Convolutions 2015:1–9.
[38] Hochreiter S. The Vanishing Gradient Problem During Learning Recurrent Neural Nets and Problem Solutions. Https://DoiOrg/101142/S0218488598000094 2011;6:107–16. https://doi.org/10.1142/S0218488598000094.
[39] He K, Zhang X, Ren S, Sun J. Identity mappings in deep residual networks. Lect Notes Comput Sci (Including Subser Lect Notes Artif Intell Lect Notes Bioinformatics) 2016;9908 LNCS:630–45. https://doi.org/10.1007/978-3-319-46493-0_38/TABLES/5.
[40] Iandola F, Moskewicz M, Karayev S, Girshick R, Darrell T, Keutzer K. DenseNet: Implementing Efficient ConvNet Descriptor Pyramids 2014.
[41] Khan U, Pao W, Sallih N. A Review: Factors Affecting Internal Two-Phase Flow-Induced Vibrations. Appl Sci 2022;12:8406. https://doi.org/10.3390/app12178406.
[42] Sohail M, Pao W, Azam H, Khan U. Two-phase Upward Flow-Induced Vibrations in U-bend under Different Orientations. J Adv Res Fluid Mech Therm Sci 2024;114:1–12. https://doi.org/10.37934/arfmts.114.1.112.
[43] Marques G, Agarwal D, de la Torre Díez I. Automated medical diagnosis of COVID-19 through EfficientNet convolutional neural network. Appl Soft Comput 2020;96:106691. https://doi.org/10.1016/J.ASOC.2020.106691.
[44] Chollet F. Xception: Deep Learning With Depthwise Separable Convolutions 2017:1251–8.
[45] Sinha D, El-Sharkawy M. Thin MobileNet: An Enhanced MobileNet Architecture. 2019 IEEE 10th Annu Ubiquitous Comput Electron Mob Commun Conf UEMCON 2019 2019:0280–5. https://doi.org/10.1109/UEMCON47517.2019.8993089.
[46] Huang Y, Li DH, Niu H, Conte D. Visual identification of oscillatory two-phase flow with complex flow patterns. Measurement 2021;186:110148. https://doi.org/10.1016/J.MEASUREMENT.2021.110148.
[47] Wang H, Wen S, He Z. Identification of flow patterns in an opaque condenser tube by distributed fiber Bragg gratings. Appl Therm Eng 2025;258:124797. https://doi.org/10.1016/J.APPLTHERMALENG.2024.124797.
[48] Sohail M, Pao W, Othman AR, Azam H, Khan MR. Regression-based prediction of flow-induced dominant vibrational frequencies in two-phase flow regimes. Ocean Eng 2024;307:118178. https://doi.org/10.1016/j.oceaneng.2024.118178.
[49] Sohail M, Pao W, Othman AR, Azam H, Khan U. Numerical Investigation of Two-Phase Flow-Induced Forces in a U-Bend Pipe: A Third-Order Response Surface of Flow Regime Dependence. Arab J Sci Eng 2025:1–24. https://doi.org/10.1007/S13369-025-10522-1/TABLES/1.
[50] Hirt CW, Nichols BD. Volume of fluid (VOF) method for the dynamics of free boundaries. J Comput Phys 1981;39:201–25. https://doi.org/10.1016/0021-9991(81)90145-5.
[51] Lee HC, Wahab AKA. Performance of different turbulence models in predicting flow kinematics around an open offshore intake. SN Appl Sci 2019;1:1–14. https://doi.org/10.1007/S42452-019-1320-8/TABLES/1.
[52] Mandhane JM, Gregory GA, Aziz K. A flow pattern map for gas-liquid flow in horizontal pipes. Int J Multiph Flow 1974;1:537–53. https://doi.org/10.1016/0301-9322(74)90006-8.